3-D Modeling of Neutron Wall Loading, Tritium Breeding Ratio, and Nuclear Heating Distribution for ARIES-ACT-DCLL Design

A. Jaber, L. El-Guebaly, L. Mynsberge

April 2012

UWFDM-1408

FUSION TECHNOLOGY INSTITUTE

UNIVERSITY OF WISCONSIN

MADISON WISCONSIN

3-D Modeling of Neutron Wall Loading, Tritium Breeding Ratio, and Nuclear Heating Distribution for ARIES-ACT-DCLL Design

A. Jaber, L. El-Guebaly, L. Mynsberge

Fusion Technology Institute
University of Wisconsin
1500 Engineering Drive
Madison, WI 53706

http://fti.neep.wisc.edu

April 2012

UWFDM-1408

Abstract

Accurate neutronic characterizations of fusion power plant designs are essential in determining their operational parameters. The neutron wall loading (NWL), tritium breeding ratio (TBR), and nuclear heating distribution are parameters that must be determined for adequate shielding and protection and fuel self-sustainability of a fusion power plant. After determining the NWL for the first wall (FW), radial builds were designed to satisfy the corresponding shielding requirements. Using the DAGMC code to couple solid-modeling geometry software with Monte Carlo radiation transport, these parameters were determined for the ARIES-ACT-DCLL design. The peak NWL values are 4.0 MW/m^2 for the inboard FW, 5.5 MW/m^2 for the outboard FW, and 2.2 MW/m^2 for the divertor. The degradation of the tritium breeding based on the addition of individual design elements to the 3-D model calculated a final TBR of 1.05. Analysis of the nuclear heating determined the energy multiplication factor to be 1.1.

I. Introduction

The ARIES team [1] has developed numerous power plants that are designed with a range of aggressive and conservative tokamaks (ACT). Three-dimensional neutronic simulations of the most recent ARIES-ACT fusion power plant designs are necessary for optimization of shielding requirements and fuel self-sustainability. The parameters that are evaluated in this report are the neutron wall loading (NWL), tritium breeding ratio (TBR) and the nuclear heating distribution. The NWL is a fusion power normalized neutron current density at the FW that enables the design of adequate radial builds and ensures proper shielding against the high-energy fusion neutrons. The TBR is a measure of how many tritium atoms are created from nuclear reactions within the blanket per tritium atom consumed by the plasma. The nuclear heating is a measure of the energy deposited by neutrons and photons in the various components surrounding the plasma.

The ARIES-ACT employs a dual-coolant LiPb (DCLL) tritium breeder, much like the most recent ARIES designs [2-5]. The LiPb serves in a configuration that allows not only breeding but also self-cooling of the blanket components. However, the ARIES-ACT-DCLL first wall (FW) is He-cooled, which serves to protect the blankets from high radiant heat and particle fluxes from the plasma. In tokamaks, it is possible to position a LiPb blanket for tritium breeding on both the inboard (IB) and outboard (OB) sides of the plasma, thereby eliminating the need for a blanket behind the divertor.

The ARIES-ACT will require the calculated TBR to be 1.05 [6] to account for margins in deficiencies and uncertainties. Generally, the margin for the calculated TBR arises from known deficiencies in nuclear data, known deficiencies in modeling, unknown uncertainties in design elements, and tritium bred in excess of the tritium consumed by D-T fusion reactions within the plasma [7]. For the ARIES-ACT, the margin totals to approximately 5%. The nuclear data uncertainty is taken to be 3%, and it arises from the ENEA experiment that validates the data for the LiPb breeder [8]. There are no uncertainties in design elements but the remaining margin arises from 1% for the known deficiencies in modeling and 1% for accounting for T bred in excess of T consumed in the plasma.

II. Methodology and Codes

A coupling of computer codes was used to perform the neutronic analysis for the ARIES-ACT-DCLL tokamak. These codes were Cubit and Directly Accelerated Geometry Monte Carlo (DAGMC). Cubit was used for the solid modeling needed to build the model to be used by DAGMC for performing the Monte Carlo radiation transport. The DAGMC code was used for the Monte Carlo simulations since it allowed neutron transport directly on a computer-aided design (CAD) model, which is incredibly useful for such complex tokamak geometries.

Cubit is a solid modeling and mesh generation software toolkit developed and released by Sandia National Laboratories [9]. Cubit provided the ability to build and prepare 3-D models necessary for CAD-based radiation transport to be used for the 3-D analysis. Cubit was required for its unique ability to detect and eliminate redundant surfaces of adjacent volumes through the use of the imprint and merge functions. Inadequate designs will cause incomplete imprinting and merging that will result in a poorly defined geometry and lost particles in the radiation transport simulation. Cubit not only gives the user the ability to create the complete 3-D geometry, but it also can group volumes and surfaces in order to assign material densities, define boundary conditions, and define desired tallies for the radiation transport simulation. Cubit provided the ability to build the model to be used by the next code, DAGMC, to perform the Monte Carlo radiation transport.

The DAGMC code [10] is a software tool developed by the Computational Nuclear Engineering Research Group (CNERG) at the University of Wisconsin-Madison that provides the ability to perform Monte Carlo radiation transport on complex 3-D geometries created by solid modeling software. This code gives the ability to translate a CAD model into a faceted 3-D geometry that can be interpreted by radiation transport software. DAGMC utilizes the radiation transport code MCNP5 [11]. By using Cubit to prepare the geometry, the user is only required to create a portion of the data cards associated with a typical MCNP5 input. The nuclear data used in this analysis is taken from Fusion Evaluated Nuclear Data Library [12].

The ARIES-ACT-DCLL is modeled as the upper half of an 11.25^{o} wedge throughout the 3-D analysis. There are 16 blanket modules that span 22.5^{o} each, thus the 11.25^{o} wedge in the CAD model represented one half of a complete blanket module. Reflecting surfaces were placed on both sides of the 11.25^{o} wedge as well as at the midplane. Thus, the 3-D model represented $1/64^{th}$ of the complete tokamak. The neutron source distribution within the plasma region was approximated using a three-nested source distribution with varying intensities (63%, 32%, and 5%) [13].

The most innovative feature of this analysis is the assessment of the degradation of individual design elements to the TBR of ARIES-ACT-DCLL blanket design. There were 15 individual simulations that measured the impact of design elements, including FW, blanket walls, cooling channels, SiC flow channel inserts (FCI), W stabilizing shell, and the assembly gap between blanket modules. The impact of varying the enrichment was determined and the reduction in TBR due to penetrations was estimated. Additionally, the FW design used in this analysis was compared to two alternative FW designs.

III. Neutron Wall Loading Results

Using Cubit to build and prepare a 3-D model in addition to DAGMC to perform Monte Carlo radiation transport on the model, neutronic simulations were performed to obtain the NWL distribution along the FW of the ARIES-ACT tokamak. Figure 1 shows the model that was used for the analysis.

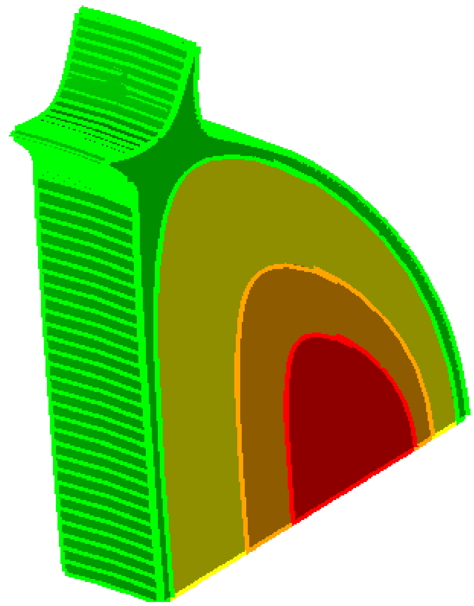

Fig. 1. 3-D ARIES-ACT tokamak model used for the NWL analysis. The FW surfaces are segmented in order to accurately obtain the NWL at various surfaces.

IIIa. Inboard and Outboard First Walls

Results were obtained for the NWL distribution along the IB and OB FW of the ARIES-ACT tokamak with a fusion power of 2767.5 MW (Figure 2). The NWL decreased as the vertical distance from the midplane increased. The peak NWL occurred at the midplane for the IB and OB FW. The IB peak NWL is 4.0 MW/m^2 and the OB peak is 5.5 MW/m^2.

IIIb. Divertor Plates

The divertor plates were segmented in order to obtain the NWL distribution along each plate. This is shown in Figure 3. As the distance from the plasma increased, the NWL decreased. As mentioned, the NWL is a measurement of current density, meaning that the angle with which the surface faces the plasma will have higher NWL. Therefore, the maximum NWL value will not necessarily occur at the lowest point for the divertor as it did with the IB and OB FW. Instead, the divertor area maximum NWL value of 2.2 MW/m^2 occurred near the middle of the dome plate at a height of 3.7 m from the midplane. Figure 4 reveals the NWL distribution along each plate of the divertor.

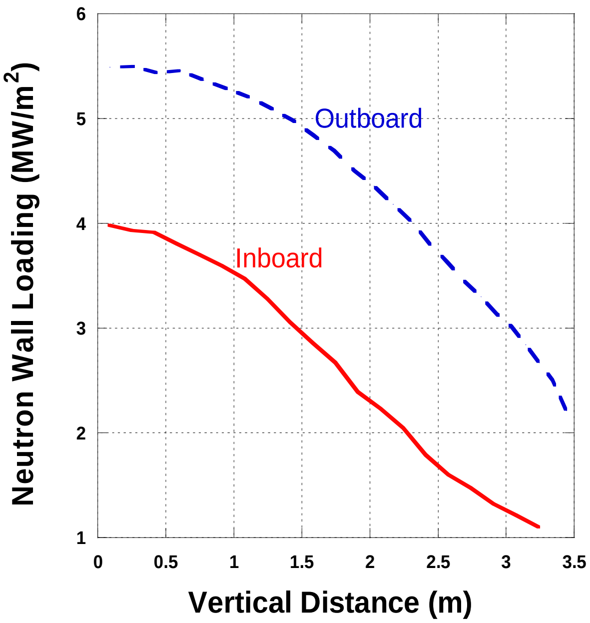

Fig. 2. IB and OB FW NWL results. The IB peak NWL is 4.0 MW/m^2 and the OB peak is 5.5 MW/m^2.

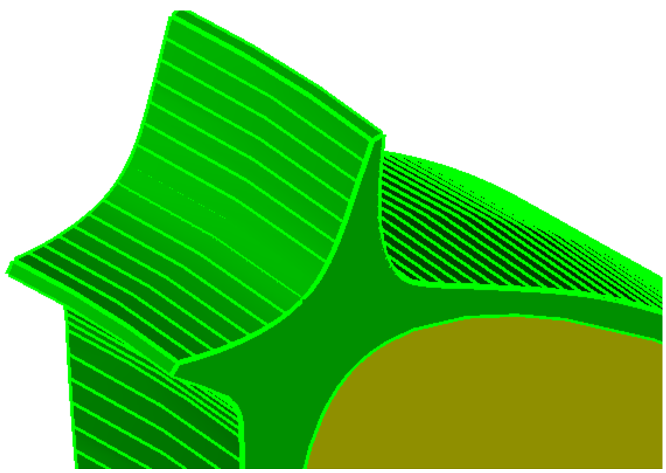

Fig. 3. The divertor area of the 3-D ARIES-ACT tokamak model used for the NWL analysis. These divertor surfaces are segmented in order to accurately obtain the NWL at various surfaces.

IV. Tritium Breeding Ratio Results

A detailed analysis of the TBR of the ARIES-ACT tokamak was performed to determine the impact of various design elements involved in creating the accurate and detailed 3-D model. Additionally, alternative FW designs were tested as well as the impact of homogenization of the blanket regions.

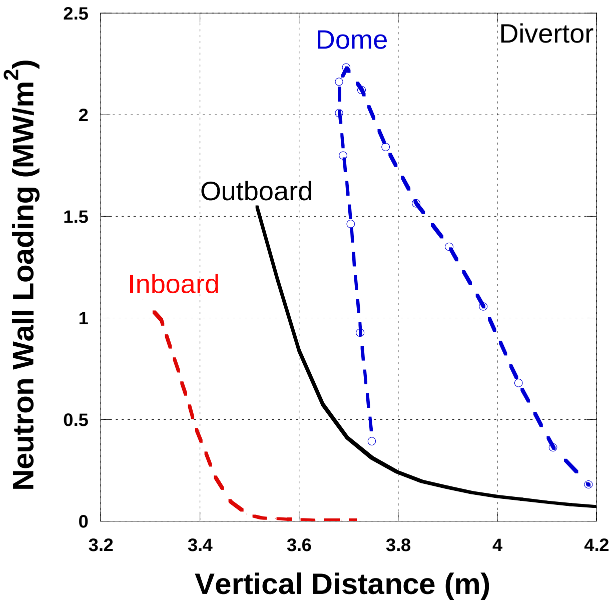

Fig. 4. Divertor NWL results. The peak NWL is 2.2 MW/m^2 and occurred near the middle of the dome plate at 3.7 m from the midplane.

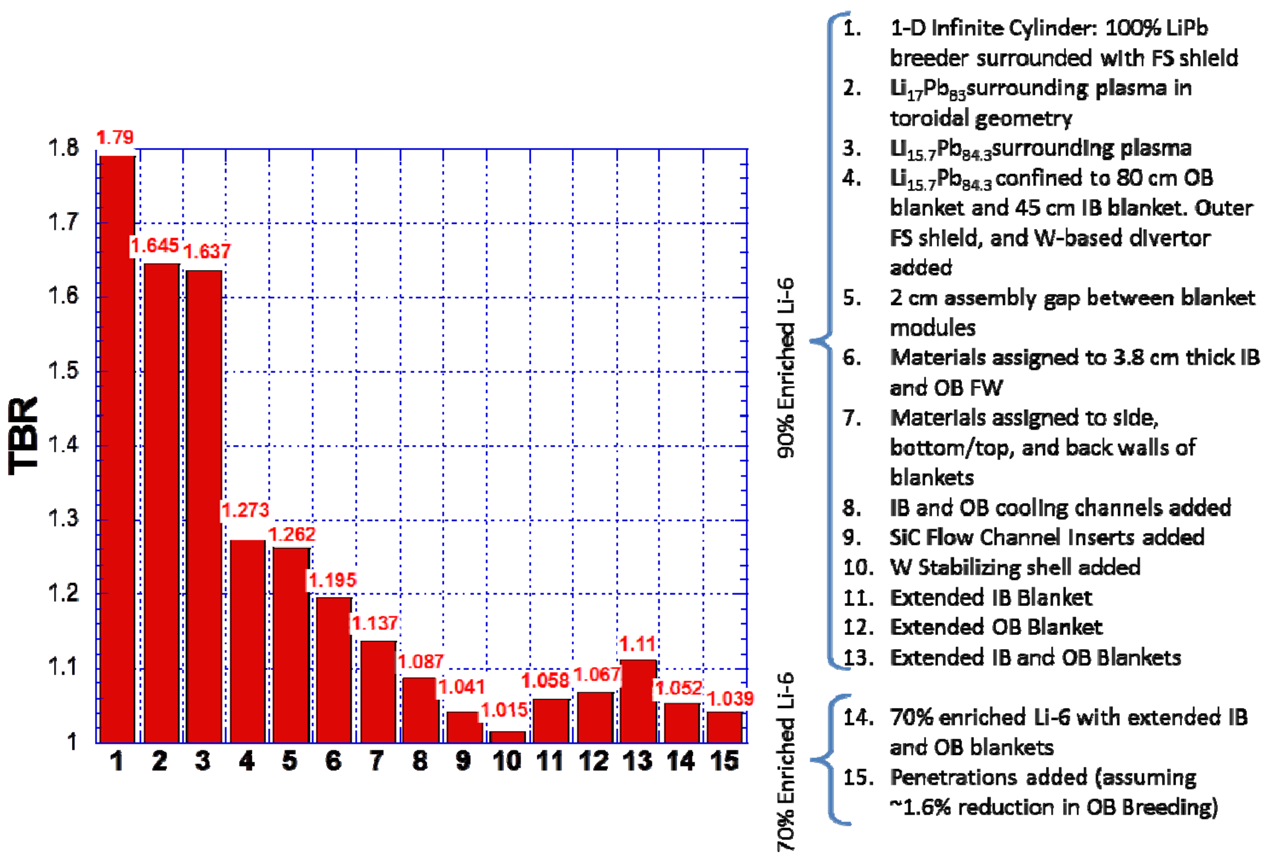

Fig. 5. This bar chart shows the reduction in TBR from 1.79 to 1.04 as a result of including the blanket details of the ARIES-ACT-DCLL model.

IVa. Step 1: Shielded 1-D Infinite Cylinder

In order to estimate the highest achievable TBR, a model of a 1-D infinite cylinder was created. The model consisted of a central neutron source represented by a cylinder of radius 75 cm surrounded by 85 cm void, 200 cm of $Li_{17}Pb_{83}$ breeder region, and 200 cm ferritic steel (FS) shield. Figure 6 illustrates the cylindrical model. The LiPb contains 90% enriched ^{6}Li. The top and bottom surfaces of the cylinder were assigned to be reflecting boundaries in order to model an infinite cylinder. A series of calculations was performed to examine the optimal shield thickness when considering neutron reflection from the FS that would enhance the breeding. Saturation occurred with a 200 cm thick shield. The TBR that corresponded to the saturation shield thickness was calculated to be 1.79 and was used as the initial reference point in the 3-D analysis as seen in Figure 5.

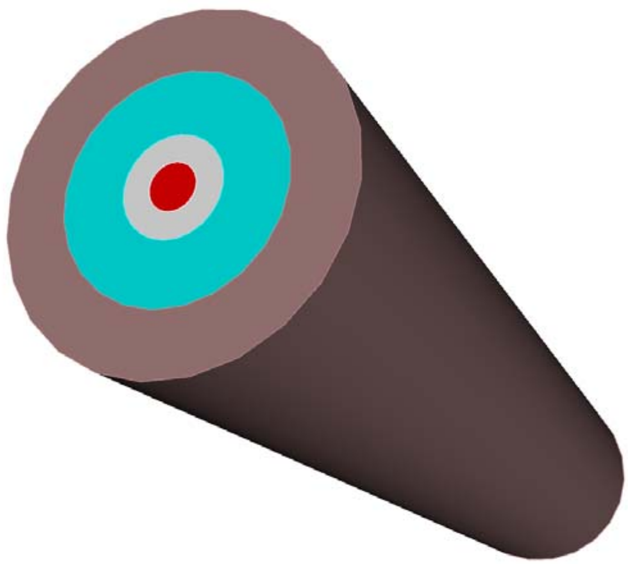

Fig. 6. Cylindrical model used to test the upper limit of breeding when using LiPb. This is an upper limit of the TBR and the first step used in the analysis. The TBR is 1.79.

IVb. Step 2: 3-D Toroidal Model

For the second calculation in the TBR analysis, the 3-D model used in the NWL calculation that consisted of the three-nested plasma surrounded by the scrapeoff layer (SOL) was used. The model was surrounded by a breeding region that was to be later redefined as the various design elements corresponding to the detailed radial build. Figure 7 illustrates the model and clearly shows the three nested plasma regions, SOL, and breeding region used for this initial calculation. The TBR was calculated to be 1.645 using a LiPb breeder composed of 17% Li and 83% Pb by atom ($Li_{17}Pb_{83}$). For these calculations and all others (unless otherwise noted), the Li contains 90% Li-6 enrichment.

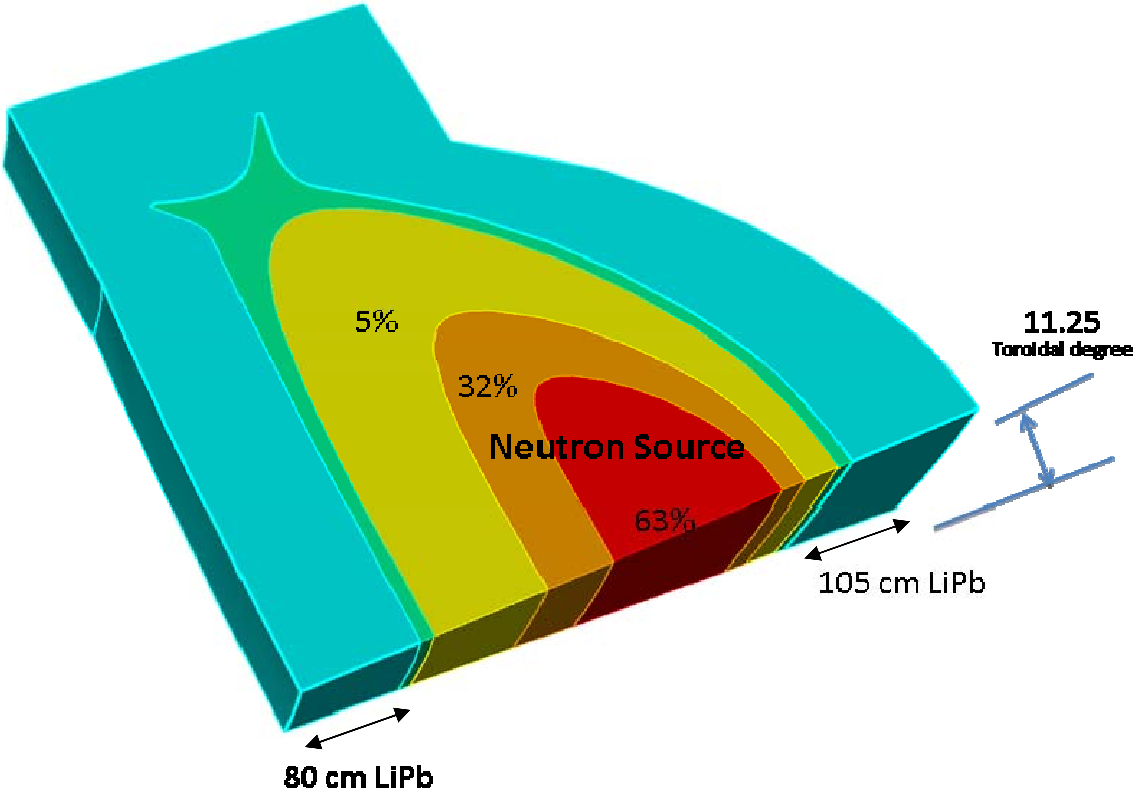

Fig. 7. 3-D CAD model of the ARIES-ACT tokamak used in determining the TBR. The plasma regions are shown in red, orange, and yellow. The SOL is colored green and the breeder is shown in light blue. The thicknesses at the midplane of the blanket region are 0.8 m on the IB and 1.05 m on the OB. The distance from the midplane to the top of the model is 4.88 m.

IVc. Step 3: Replacing $Li_{17}Pb_{83}$ with $Li_{15.7}Pb_{84.3}$

Traditionally, the $Li_{17}Pb_{83}$ breeder [14] has been used throughout fusion design studies. In recent decades, European scientists have shown the lead-rich eutectic of the LiPb system lies at 15.7% Li and 84.3% Pb [15]. Therefore, the next calculation was performed using the same model as in the previous step but with atom percentages of 15.7% Li and 84.3% Pb for the LiPb breeder. With this lower Li composition in the LiPb, the TBR drops to 1.637. The $Li_{15.7}Pb_{84.3}$ is used in the remainder of the analysis.

IVd. Step 4: $Li_{15.7}Pb_{84.3}$ Confined to Blanket

The next step in the TBR analysis was to confine the breeder to IB and OB blankets. A preliminary estimate supports a 45 cm thick IB blanket and 80 cm thick OB blanket consisting of 2 segments, 40 cm thick. Materials were assigned to the surrounding outer shield and divertor plates. The outer shield was 35 cm thick on IB, 20 cm thick on the OB, and 65 cm thick beyond the divertor. The divertor plates are 7.7 cm thick. Figure 8 is a schematic of the IB and OB radial build.

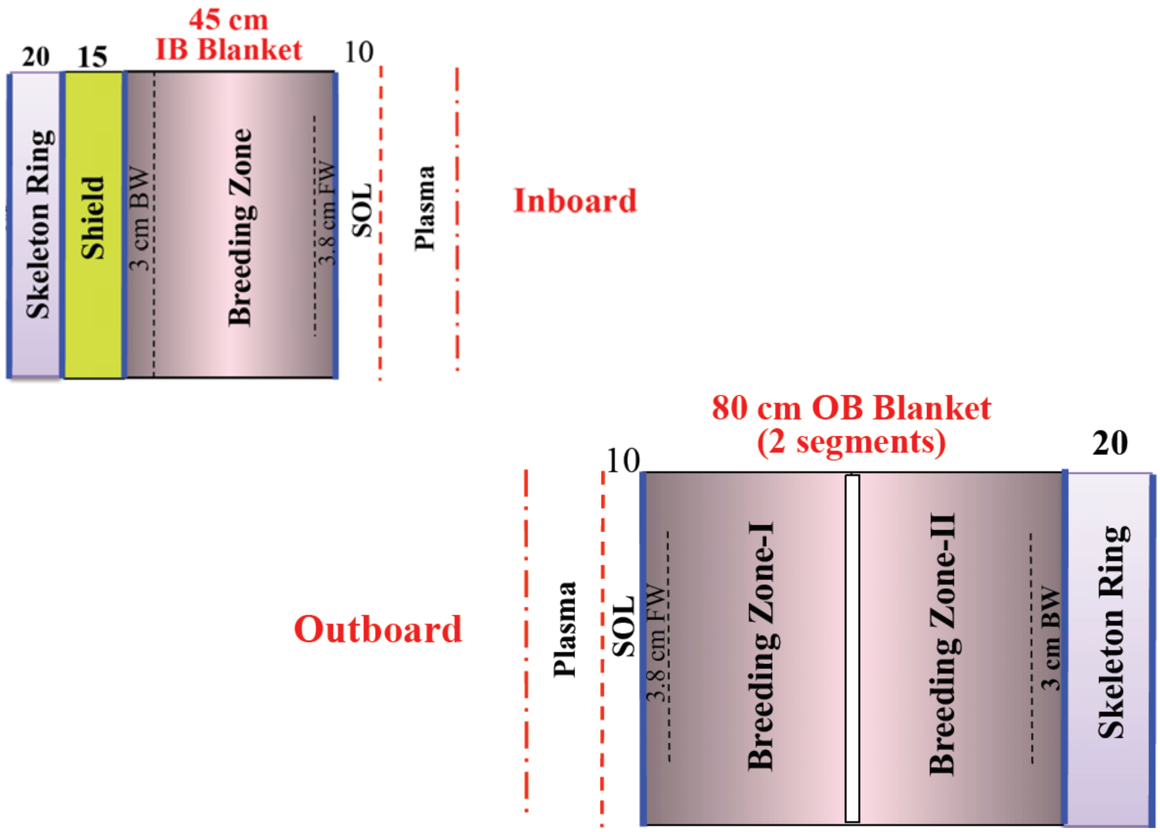

Fig. 8. This figure shows a schematic of the IB and OB radial build.

The outer shield was given a composition of 15% F82H, 75% Borated FS, and 10% He. The divertor plates were given a composition of 8% W, 28% W-TiC, 11% ODSFS, and 53% He. Figure 9 shows the 3D model used for this analysis. The TBR reduced to 1.273 due to confining the IB and OB blankets.

IVe. Step 5: Adding Assembly Gaps

Following the confinement of the breeder to the blanket regions, a 2 cm radial-poloidal gap was modeled on one side of the 11.25^{o} ARIES-ACT wedge. The gap is a necessary design element between adjacent blanket modules to allow for thermal expansion, neutron induced swelling and the removal of blanket modules during maintenance. Figure 10 shows the gap included in the model colored in purple. Since half of the blanket module is being modeled, the gap in Figure 10 is 1 cm wide. The TBR degrades slightly to 1.262 with the addition of the assembly gap.

IVf. Step 6: Materials Assigned to FW

Next, materials were assigned to the IB and OB FW. The 3.8 cm thick FW was defined as 8% ODSFS, 27% F82H, and 65% He. Figure 11 shows the IB and OB FW colored in black. All other design elements maintain the same material definition as in the previous step. This caused the TBR to drop to 1.195.

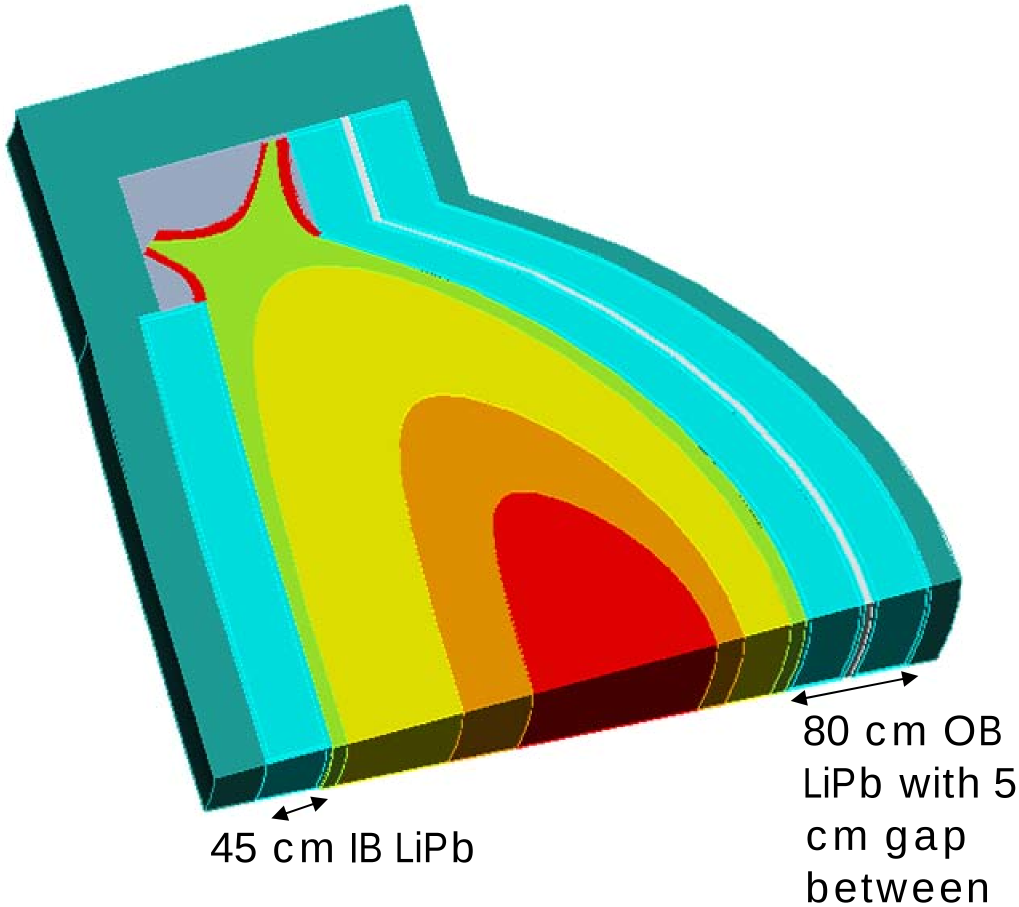

Fig. 9. 3-D CAD model of the ARIES-ACT tokamak used in determining the TBR. The breeder is confined to the blankets shown in light blue. The thicknesses at the midplane of the blanket region are 45 cm on the IB and 40 cm for each OB blanket segment. The divertor plates are colored red. The outer shield is colored teal.

IVg. Step 7: Side/Top/Back Walls Added

Each of the blanket regions contains side, top, front and back walls that will degrade the TBR, and the next step was to include the blanket walls for each blanket. The thickness of the blanket walls is detailed in Table 1. Figure 12 shows a midplane cross section of the IB and OB blanket with the blanket walls defined and colored in dark blue. The TBR drops to 1.137 with the addition of the blanket walls.

Table 1. Blanket Wall Thicknesses

	IB Blanket (cm)	OB Blanket I (cm)	OB Blanket II (cm)
Side wall	3.5	3.5	3.0
Top wall	3.5	3.5	3.0
First/Front wall	3.8	3.8	3.0
Back wall	3.0	3.0	3.0

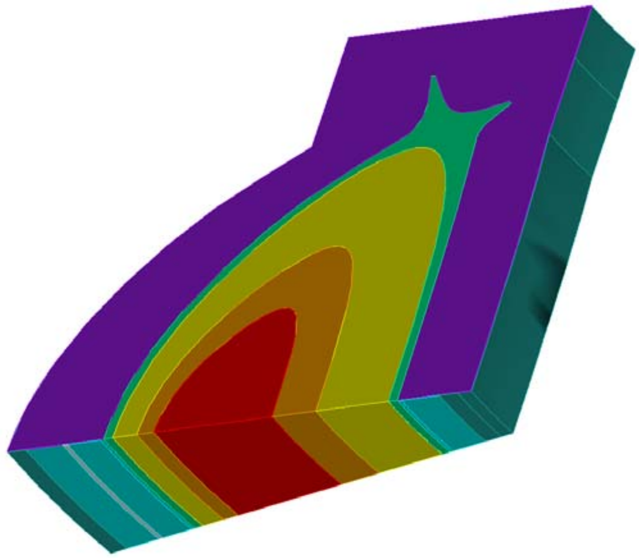

Fig. 10. This figure shows the addition of the assembly gap into the 3D model. The assembly gap is colored purple and extends over all components. The plasma region remains continuous toroidally.

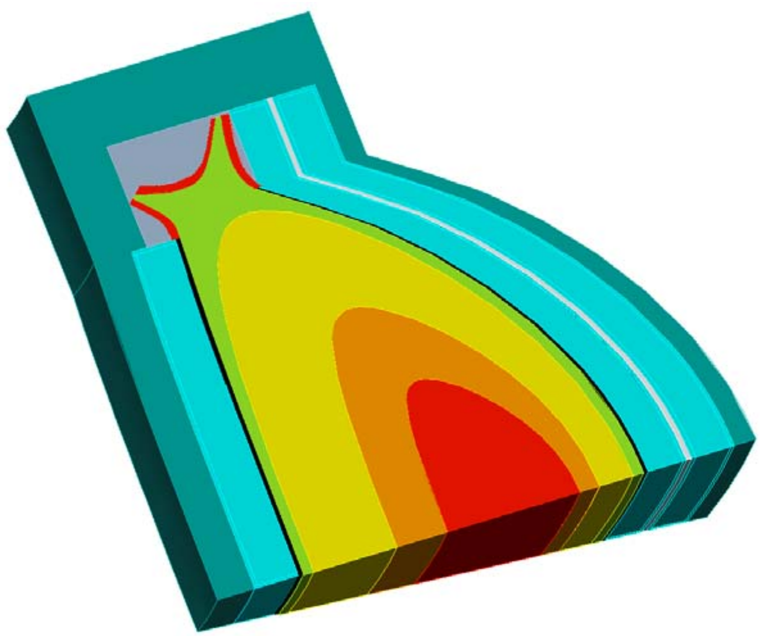

Fig. 11. An isometric image of the 3-D tokamak. The IB and OB FW are shown in black.

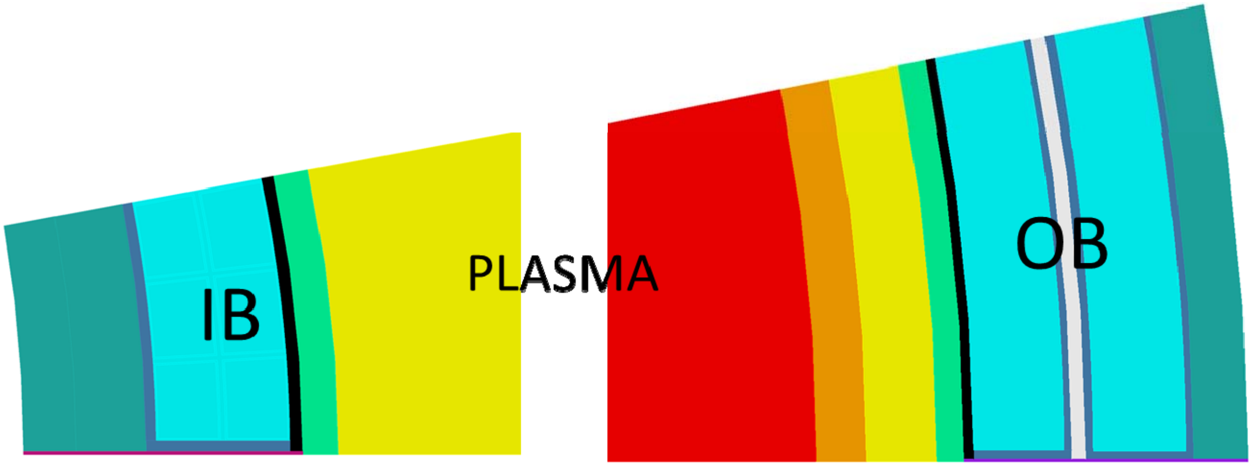

Fig. 12. Midplane cross section showing the addition of the side and back blanket walls that are colored dark blue.

IVh. Step 8: Cooling Channels Added

After the addition of the blanket walls, the cooling channels were added to model the channels in which the LiPb breeder will be contained. Each IB blanket module is divided into 12 channels, so the IB blanket in the model was divided into six channels. The cooling channels have material compositions of 58% F82H and 42% He. As was mentioned, this model is half of a complete module so half of a cooling channel wall on the IB and half of the LiPb breeder channels on the OB were modeled at the side opposite to the assembly gap. This design element can be seen in the midplane cross sections shown in Figure 13. The TBR with the cooling channels added is reduced to 1.087.

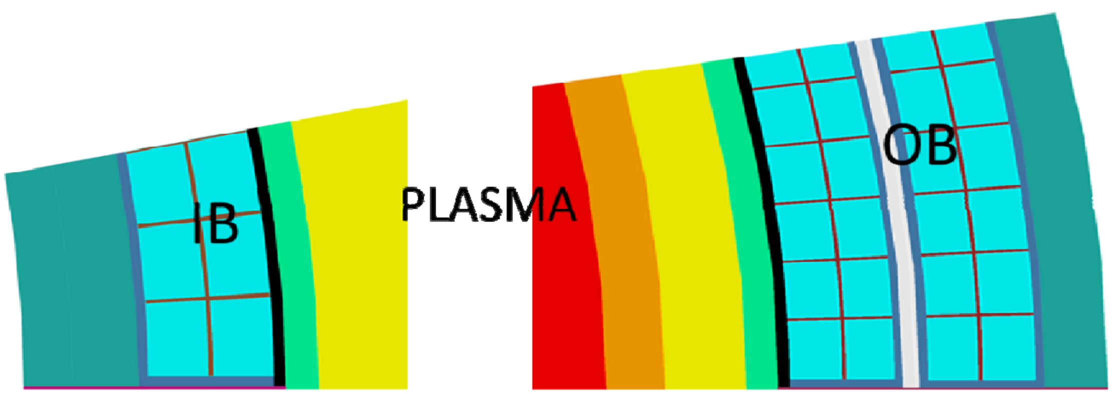

Fig. 13. This figure shows the addition of the cooling channel walls on the IB side of the 3-D model. The channels are colored brown.

IVi. Step 9: SiC FCI Added

The next step quantifies the TBR degradation from the addition of the SiC FCI, which agrees with previous analyses regarding its effect on the TBR [16,17]. All FS walls and cooling channels are lined with 0.5 cm thick SiC FCI as shown in Figure 14. The SiC FCI serves as a thermal and electric insulator to the FS structures within the blanket. The FCIs are composed of 46% dense SiC based on the Ultramet type [18]. The TBR falls to 1.041, which is below the required calculated TBR value of 1.05 even before the addition of the W stabilizing shells and penetrations.

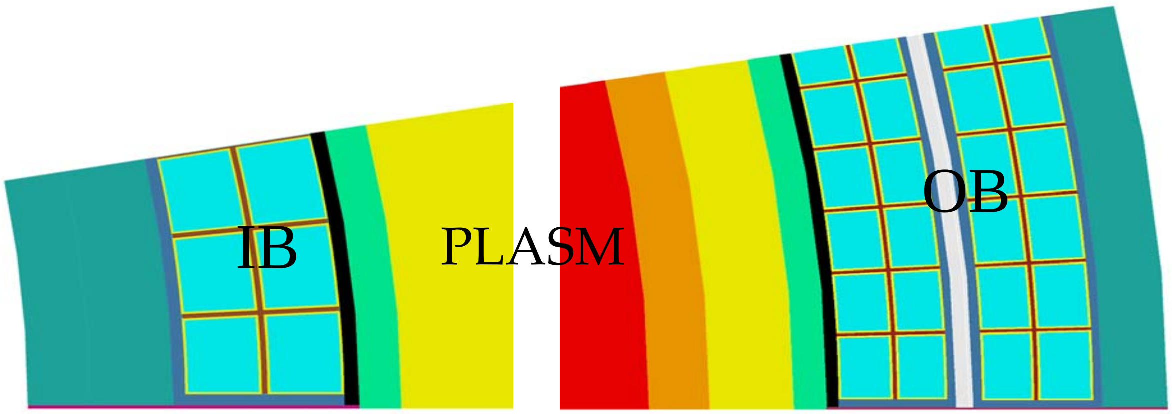

Fig. 14. This figure shows the addition of the SiC Flow Channel Inserts. The FCIs are colored in yellow and enclose each LiPb channel.

IVj. Step 10: Adding Stabilizing Shells

The TBR degradation due to the addition of the W stabilizing shells was also determined. The W shell was placed at strategic locations behind the IB blanket and between the two OB blanket segments. The IB vertical stabilizing (VS) shell was 4 cm thick and was placed between 135^o and 145^o with respect to the center of the magnetic axis at 6.3 m from the tokamak center column. The OB VS shell was 4 cm thick and was placed between 55^o and 85^o with respect to the center of the magnetic axis. And finally the OB Kink shell was 1 cm thick and placed between 0^o and 45^o with respect to the center of the magnetic axis. The OB plates of the W shell were placed in the 5 cm gap between the OB blankets. The W shell is shown in Figures 15 and 16. The TBR is reduced to 1.015 due to the addition of the shells.

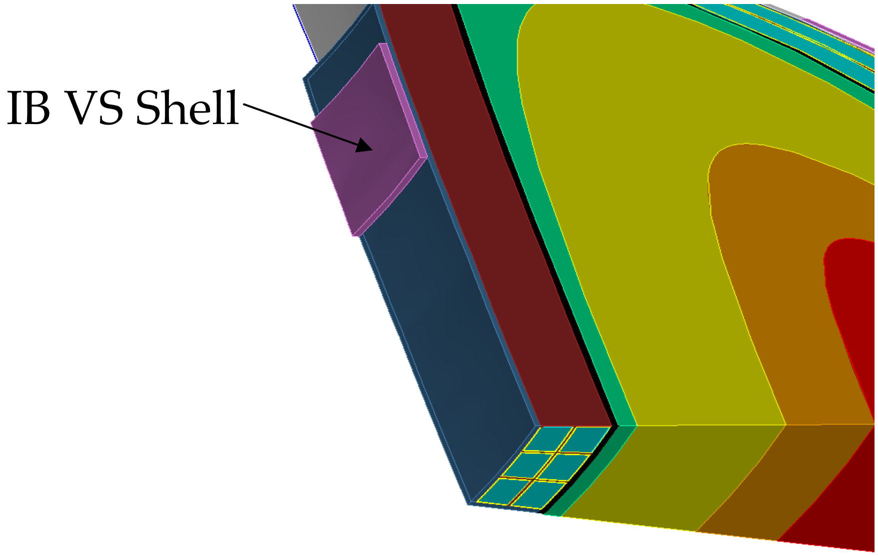

Fig. 15. Cutaway isometric that shows the addition of the W VS shell on the IB side of the 3-D model. The W shell is colored violet.

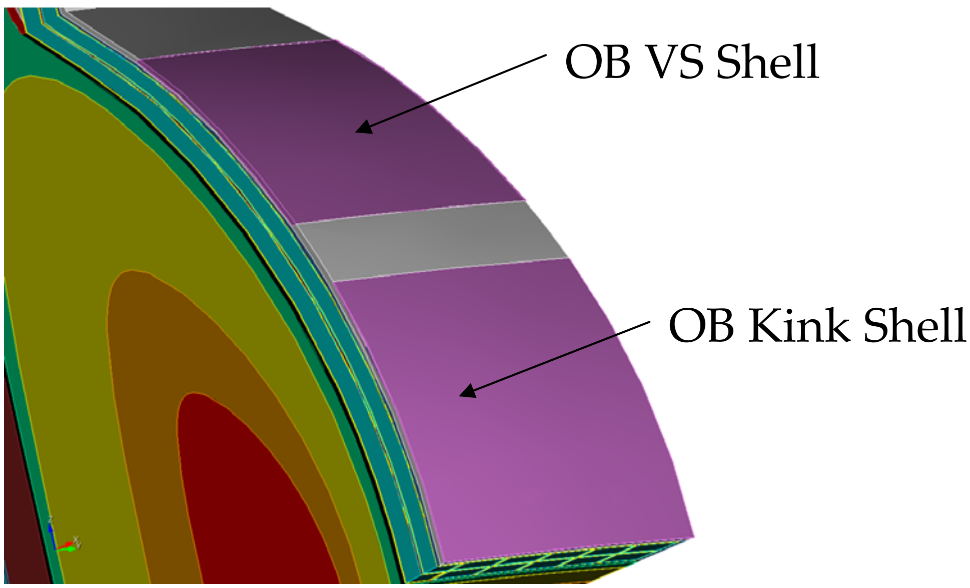

Fig. 16. Cutaway isometric that shows the addition of the W shells on the OB side of the 3-D model. The W shell is colored violet.

IVk. Step 11: Extend IB Blanket

After the addition of the W shells, the TBR fell below the value needed to account for uncertainties in the breeding margin [6] and the desire to operate at lower Li-6 enrichment. More breeding regions became necessary to increase the total TBR so extensions to the IB and OB blankets were considered. First, the IB blanket was extended as shown in Figure 17. The extended IB blanket increased the TBR to 1.058.

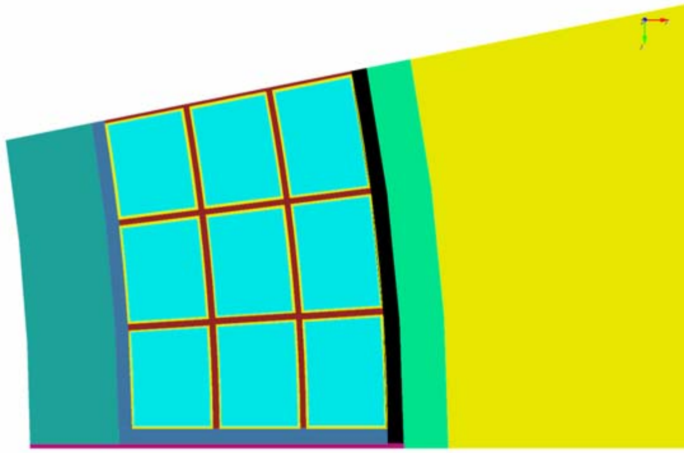

Fig. 17. IB midplane cross section that shows the extended IB blanket. The total number of IB channels in the model increased from six to nine.

IVl. Step 12: Extend OB Blanket

The TBR from extending the IB blanket was too low for Li-6 enrichment variation so extending the OB blanket was subsequently examined. The total number of channels on the OB increased from 44 to 55 for the 1/16th module. The 1/32nd model of the OB blankets is shown in Figure 18. The IB blanket was not extended during this step in order to examine the increase in TBR for the extended OB blanket only. The TBR increased to 1.067 with the extended OB blanket.

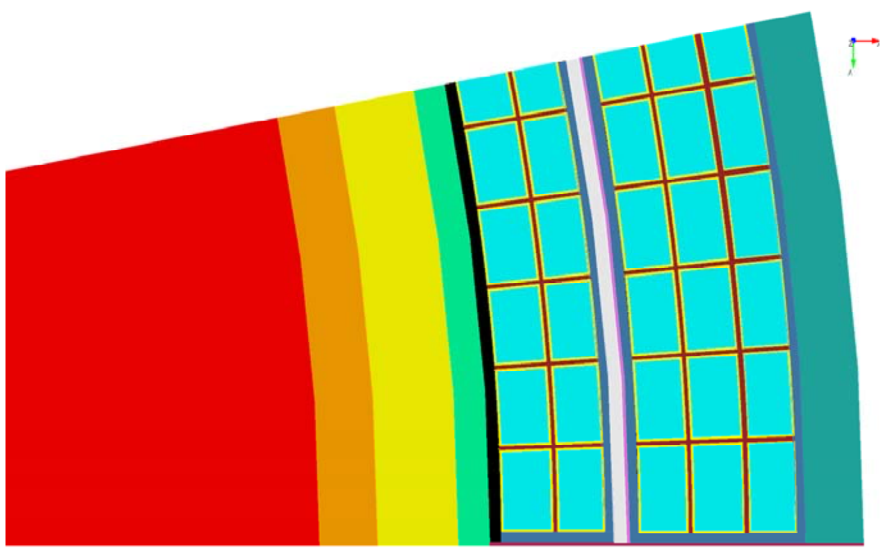

Fig. 18. OB midplane cross section that shows the extended OB blanket.

IVm. Step 13: Both IB and OB Blankets Extended

In order to obtain adequate breeding and also allow for reduced Li-6 enrichment below 90%, both blankets must be extended. The TBR due to both IB and OB blanket extensions was modeled for this step. With a total of 18 IB and 55 OB channels for a 1/16th sector, the TBR increased to 1.11. An isometric of the complete model is shown in Figure 19.

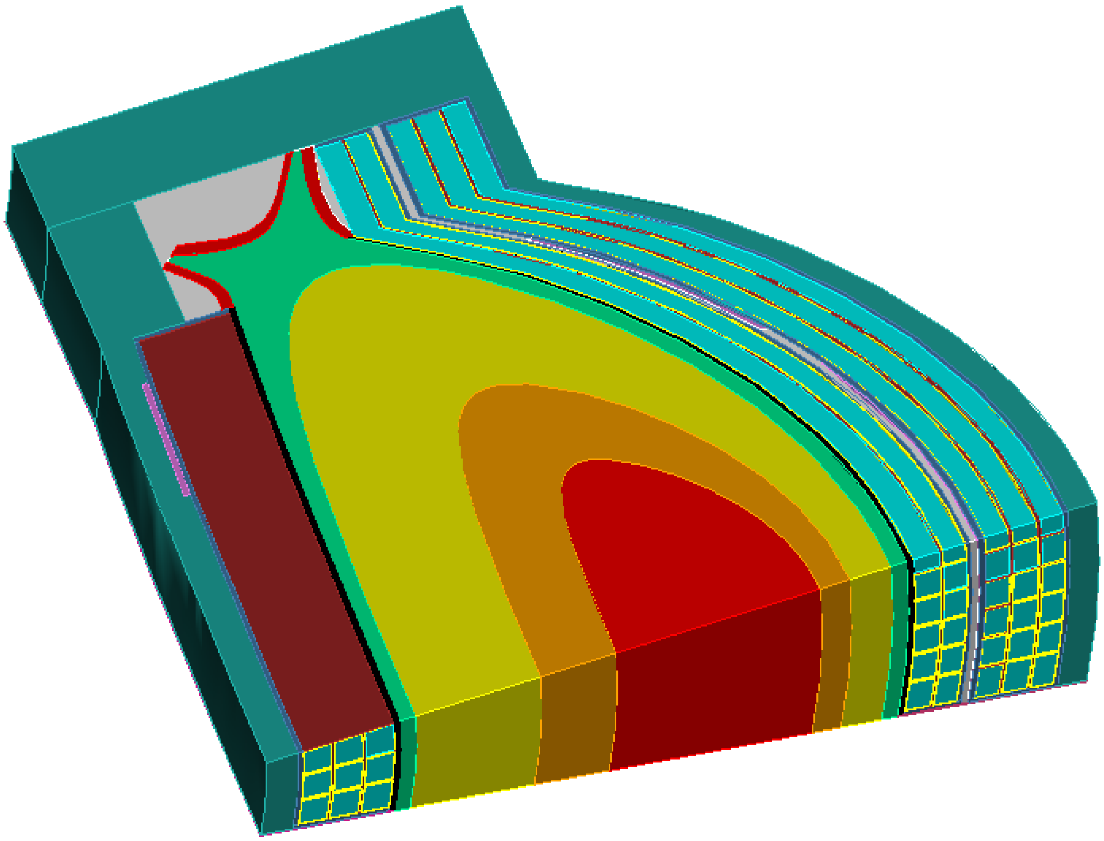

Fig. 19. Isometric of final 3-D model used for TBR analysis.

IVn. Step 14: Varying Li-6 Enrichment

The enrichment of the Li-6 in the LiPb breeder was varied to determine if it is possible to operate the tokamak at lower enrichments. Several enrichments were used to evaluate the trend. The TBR trend due to varying the Li-6 enrichment is shown in Figure 20. The TBR degradation due to lower enrichment was calculated in this step. The TBR was reduced to 1.052 with 70% Li-6 enrichment.

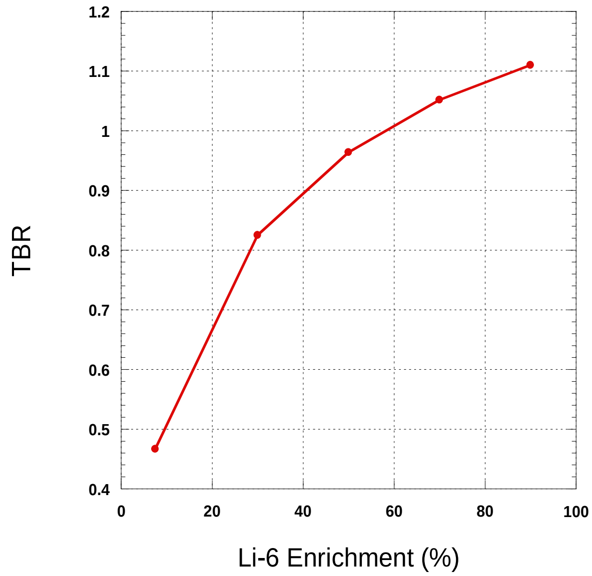

Fig. 20. Change in TBR of the extended blanket design with varying Li-6 enrichment within the LiPb breeder.

IVo. Step 15: Adding Penetrations

Finally, OB penetrations for diagnostics and plasma control were considered. A total OB penetration FW area of 5.7 m^2 was used [6]. The total OB FW area was 350 m^2. The penetration area was converted to a fraction of the total FW area and multiplied by the OB contribution to the TBR. This yielded an approximate degradation of the TBR due to the addition of the penetrations in the ARIES-ACT design. The TBR decreased to 1.039 in this step.

IVp. Radial and Poloidal Distribution

The radial distribution of the TBR was determined in order to obtain the breeding profile within the blankets. Figure 21 shows the distribution of the TBR in each channel along with the relative statistical error of each value as reported by the DAGMC code. The TBR contribution from each channel decreases with increasing distance from the plasma. The OB blanket contributes approximately 73% to the total breeding while the IB blanket provides the remaining 27%.

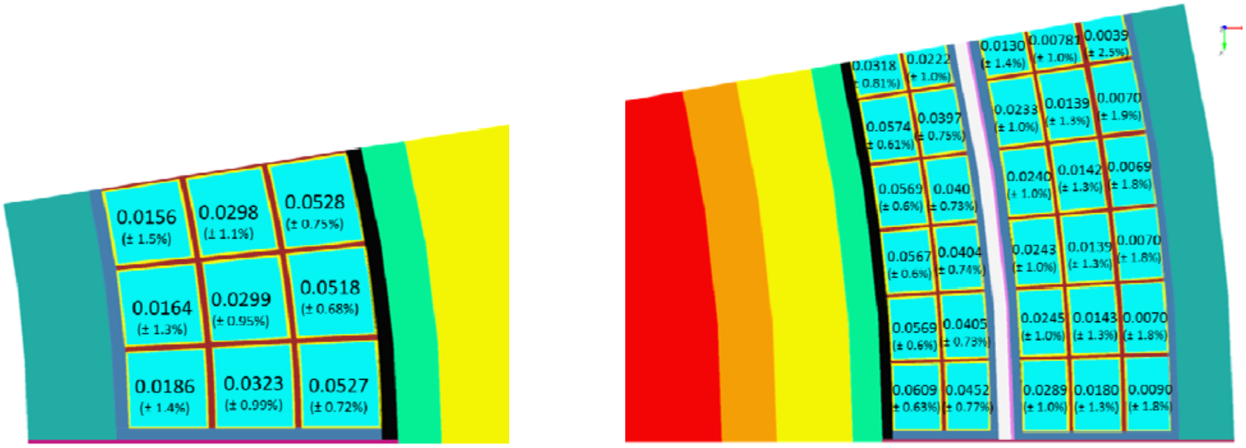

Fig. 21. Radial distribution of TBR and relative error of each value. This figure shows the equal contributions of the channels located at the same radial distance from the plasma.

The poloidal distribution was also evaluated by calculating the TBR at various vertical distances from the midplane. The LiPb channels were segmented in 20 cm intervals from the midplane in order to determine the poloidal distribution. The segmentation of the channels is shown in Figure 22 and the results are shown in Figure 23. The results confirm that the TBR is highest at the midplane where the neutron flux peaks. The effect of the W stabilizing shell is apparent in the regions where the TBR decreases for OB3, OB4, and OB5 around the midplane due to the Kink shell and at distances of 1.9 m and 3.5 m due to the VS shell. A tetrahedral mesh was created over the LiPb channels to obtain a fine distribution of the TBR. Figures 24 and 25 show the fine mesh TBR results.

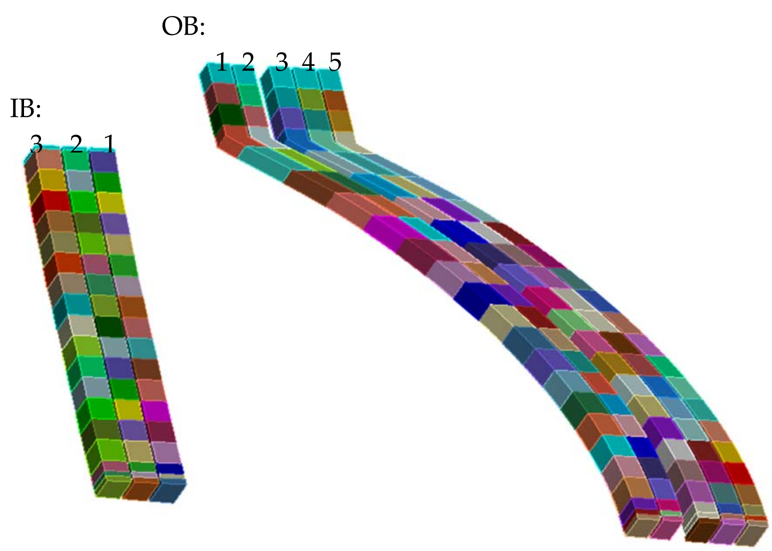

Fig. 22. Poloidal segmentation of the blanket channels to obtain the distribution of the TBR.

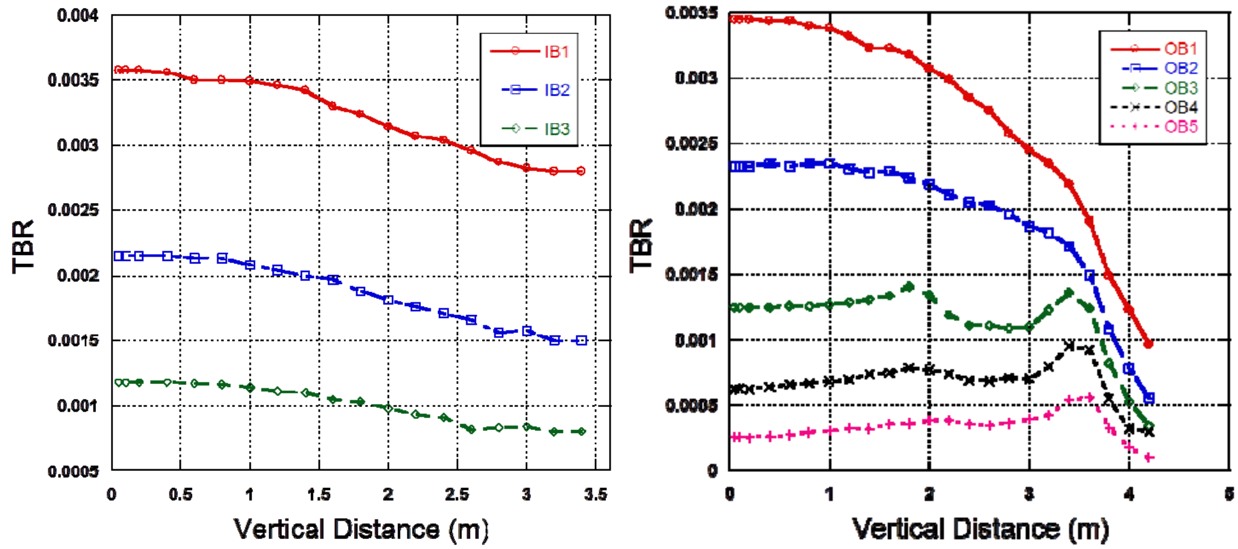

Fig. 23. Results from poloidal distribution anaylsis of breeding in IB and OB blankets.

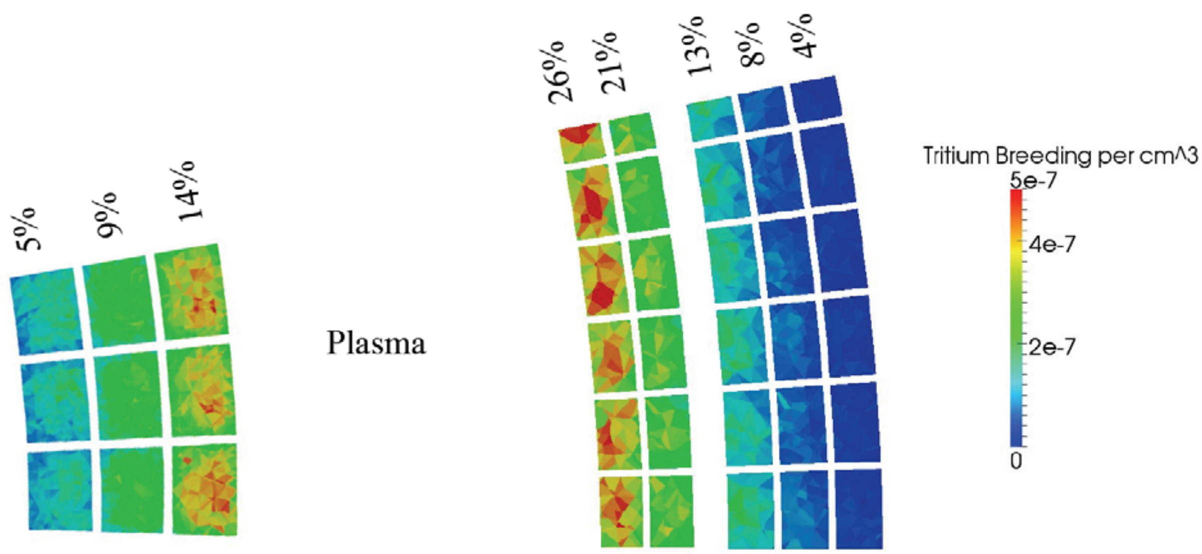

Fig. 24. A radial/toroidal slice of the breeding distribution within the IB and OB blankets.

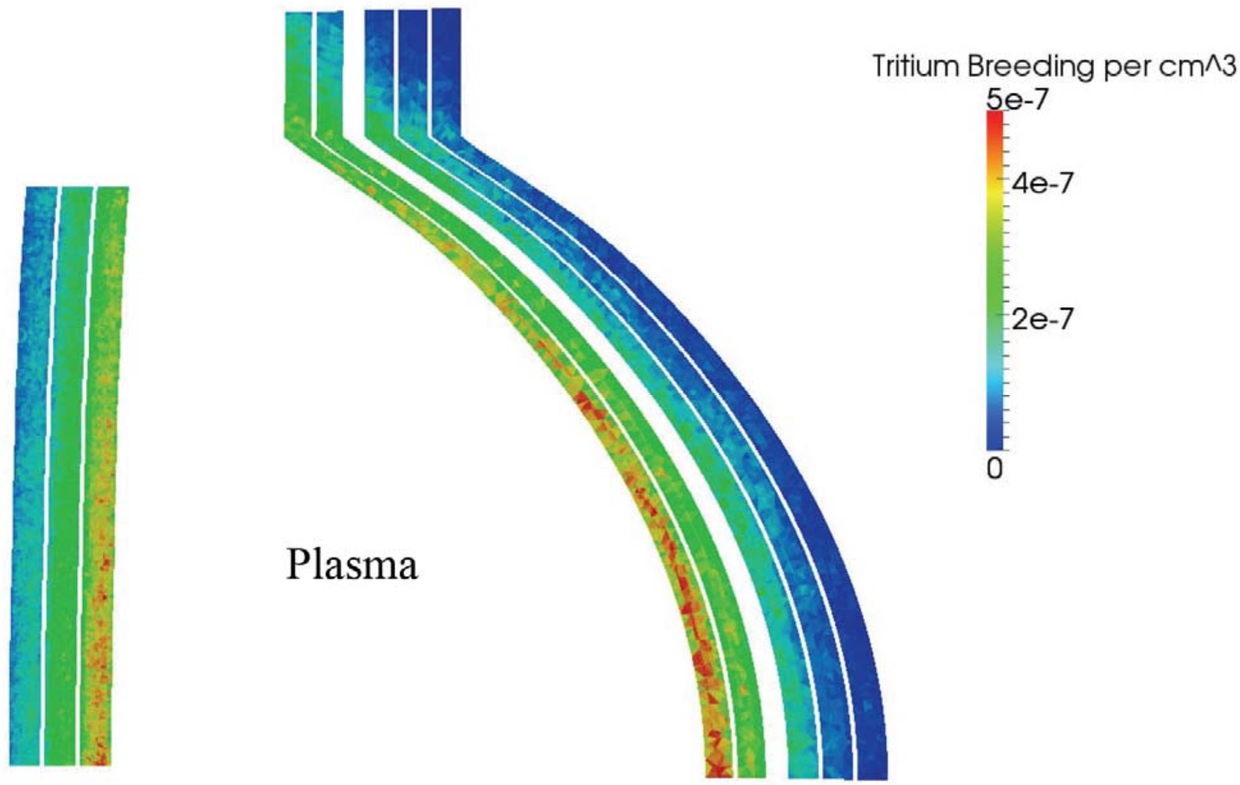

Fig. 25. A poloidal slice of the breeding distribution within the IB and OB blankets.

IVq. Alternative FW Designs

Two alternative first wall designs were explored to study the effect of the design changes on the TBR. The first alternative FW design was a FS/W-based design and had a composition of 8.2% W, 8.3% ODSFS, 22.4% F82H, and 61.1% He. The FW composition was modified in the model at Step 10 described earlier. This FW composition yielded a TBR of 1.0157, which is quite comparable to the FS-based FW used throughout the previous analysis as seen in Figure 26.

The second alternative FW design was a FW similar to that of ITER. The thickness of the FW was increased from 3.8 cm to 7.2 cm. The composition of the ITER-like FW was 25% F82H, 26% Cu, 14% Be, and 35% He (replacing water). This FW design yielded a TBR of 0.9466, much lower than the reference FW design shown in Figure 27.

IVr. Blanket Homogenization

The effect of homogenization of the blanket regions on TBR was examined. Table 2 shows the exact homogenized compositions of the blanket regions. The exact homogenized composition had a TBR value of 1.039, which is almost the same as that of the detailed blankets within statistical error (±1%). This comparison is shown in Figure 28.

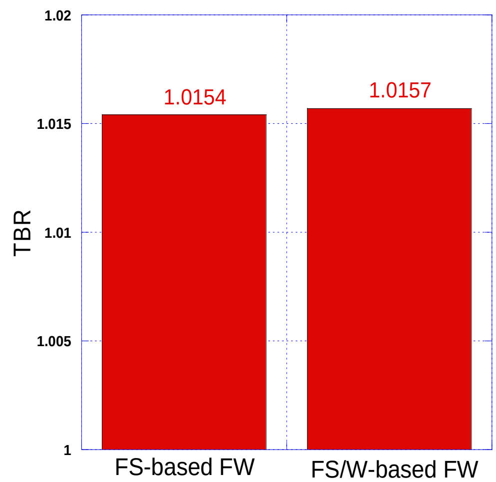

Fig. 26. Comparison of the TBR for FS-based FW and FS/W-based FW.

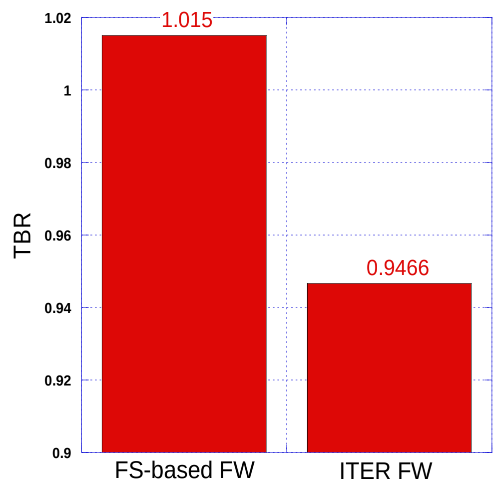

Fig. 27. Comparison of the TBR of the FS-based FW and the ITER-like FW design with He replacing water.

Table 2. Exact Homogenized Compositions of the Blanket Regions

	IB Blanket	OB Blanket I	OB Blanket II
LiPb	73.1%	71.3%	66.95%
Cooling Channels	7.5%	8.87%	7.84%
FCI	7.45%	8.36%	7.48%
Back wall	6.57%	8.17%	17.73% (all walls)
Side/Top walls	5.38%	3.3%	-

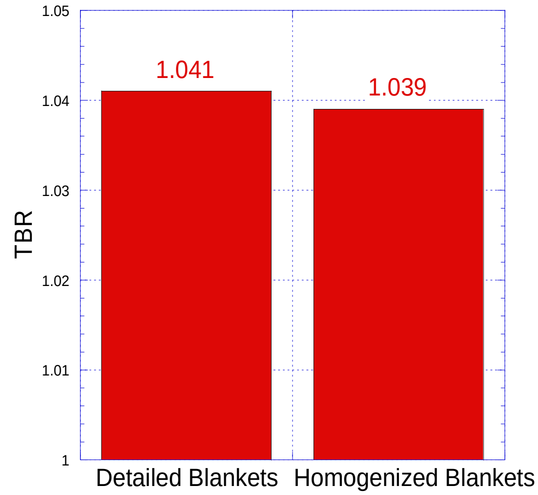

Fig. 28. This figure compares the TBR of the detailed blanket model and a homogenized blanket model.

V. Nuclear Heating Distribution Results

Breaking down the ARIES-ACT-DCLL into individual sections allowed for a complete nuclear heating analysis. The value of heating in each section was used to obtain details on the thermal hydraulic analysis and eventually the kind of thermodynamic stresses the system is subjected to during operation. The total fusion power of the tokamak was 2767.5 MW.

Va. 1/16th Tokamak Nuclear Heating

For this analysis, the 3-D model was divided into a 1/64th module as explained in Section II. The heating result was then multiplied by four to obtain the heating in a 1/16th total slice of the module. Table 3 gives a simple breakdown of the heating for a fusion power of 2767.5 MW and then a more detailed analysis is examined in Table 4.

Table 3. Broad Breakdown of Nuclear Heating in 1/16th Module

Nuclear Heating (MW)	**Inboard**	**Outboard**	**Divertor**	**Total**
FW/Blanket	33.29	100.42	-	133.72
Divertor Plates	-	-	2.22	2.22
Stabilizing Shells	0.29	4.80	-	5.09
Shield	1.45	1.27	11.32	14.04
Total	35.03	106.49	13.54	155.06

Table 4. Detailed Breakdown of Nuclear Heating in 1/16th Module

Inboard Nuclear Heating (MW)	
65 cm Thick IB Blanket:	
3.8 cm FW	3.18
58.2 cm Breeding Zone	
LiPb Flow Channels	27.29
FS/He Cooling Channels	0.97
SiC Flow Channel Inserts (FCI)	1.1
Total	29.37
3 cm Back Wall	0.13
3.5 cm Side Wall	0.43
3.5 cm Top/Bottom Walls	0.18
4 cm VS Shell	0.29
IB Shield	1.45
Total IB	35.03
Outboard Nuclear Heating (MW)	
40 cm Thick OB-I Blanket:	
3.8 cm FW	7.42
33.2 cm Breeding Zone	
LiPb Flow Channels	64.63
SiC FCI	3.51
FS/He Cooling Channels	3.16
Total	71.3
3 cm Back Wall	1.8
3.5 cm Side Wall	0.72
3.5 cm Top/Bottom Walls	0.02
Stabilizing Shells:	
1 cm Kink Shell	1.27
4 cm VS Shells	3.53
60 cm Thick OB-II Blanket:	
3 cm FW	1.51
54 cm Breeding Zone	
LiPb Flow Channels	16.54
SiC FCI	0.35
FS/He Cooling Channels	0.38
Total	17.27
3 cm Back Wall	0.09
3 cm Side Wall	0.28
3 cm Top/Bottom Walls	0.01
OB Shield	1.27

Total	106.49
Divertor Nuclear Heating (MW)	
Upper Divertor:	
7.7 cm W-based Divertor Plates:	
Inner Plate	0.19
Dome	0.56
Outer Plate	0.36
Divertor Shield	5.66
Lower Divertor:	
7.7 cm W-based Divertor Plates:	
Inner Plate	0.19
Dome	0.56
Outer Plate	0.36
Divertor Shield	5.66
Total	13.54

Table 5. Broad Breakdown of Nuclear Heating in Full ARIES-ACT-DCLL Design

Nuclear Heating (MW)	**Inboard**	**Outboard**	**Divertor**	**Total**
FW/Blanket	532.64	1606.81	-	2139.45
Divertor PLates	-	-	35.52	35.52
Stabilizing Shells	4.66	76.73	-	81.39
Shield	23.26	20.24	181.10	224.60
Total	560.55 (22%)	1703.79 (69%)	216.62 (9%)	2480.96

Vb. Full Tokamak Nuclear Heating

To find the full module's nuclear heating, all the data were multiplied by 16 (see Table 5). Adding up all the individual section's heating results in 2481 MW. Dividing the total heating by the neutron power (2767.5 MW x 0.8), an energy multiplication factor of 1.12 was found.

Table 6. Thermal Power Split Between He and LiPb Coolants

Thermal Power (MW_{th})	He	LiPb	Total
Surface Heating	674*	---	674
Recovered Power from Div Pumping	26*	---	26
Recovered Power from Blanket Pumping	~8*	~8*	16
FW	170	---	170
Breeding Zones and Walls	236	1815	2051
Divertor	36	---	36
Shields	224	---	224
Leakage from LiPb to He	~ +100	~ -100	0
Total	1474 (46%)	1723 (54%)	3197

* Oct. 2011 Strawman

VI. Thermal Power Split Between He and LiPb Coolants

Based on Table 4, we evaluated the thermal heat loads to the helium and LiPb coolants with input from the October 2011 ARIES Systems Code Strawman on the surface heating to the divertor and FW. The split between the He and LiPb loads is an essential parameter to the power conversion system and also to the ARIES Systems Code for the purpose of costing the He and LiPb heat transfer/transport system. The distribution of power is summarized in Table 6. Most of the divertor and blanket He and LiPb pumping powers are recovered by the helium and LiPb coolants as thermal power. Approximately 100 MW of heating leaks through the SiC insulator from the hotter LiPb to the colder He of the cooling channels and walls. The end result is 46:54 for the He:LiPb thermal power ratio.

VII. Conclusions

State-of-the-art tools were utilized to assess operational parameters of the ARIES-ACT-DCLL tokamak. The DAGMC code was used to couple solid-modeling software with a Monte Carlo radiation transport code in order to effectively perform analysis on the complex tokamak geometry with fine details of various design elements of the blanket regions. The results reveal that the ARIES-ACT-DCLL design not only satisfies the ARIES breeding requirements of calculated TBR of 1.05 but also the effects of individual design components on the degradation of overall TBR. In addition, the nuclear heating analysis revealed an energy multiplication factor of 1.12 and a He:LiPb thermal power ratio of 46:54 for the DCLL design.

Acknowledgment

This work was performed under the auspices of the U.S. Department of Energy (contract # DE-FG02-98ER 54462).

References

1. The ARIES Project: http://aries.ucsd.edu/ARIES/.

2. F. NAJMABADI and the ARIES Team, "Overview of the ARIES-ST Spherical Torus Power Plant Study," *Fusion Engineering and Design*, **65**, 143 (2003).

3. F. NAJMABADI, A.R. RAFFRAY, S. ABDEL-KHALIK, L. BROMBERG, L. CROSATTI, L. EL-GUEBALY et al., "The ARIES-CS Compact Stellarator Fusion Power Plant," *Fusion Science and Technology*, **54**, No. 3, 655 (2008).

4. F. NAJMABADI, A. ABDOU, L. BROMBERG, T. BROWN, V.C. CHAN, M.C. CHU, F. DAHLGREN, L. EL-GUEBALY et al., "The ARIES-AT Advanced Tokamak, Advanced Technology Fusion Power Plant," *Fusion Engineering and Design*, **80**, 3 (2006).

5. S. MALANG, A.R. RAFFRAY, and N.B. MORLEY, "An Example Pathway to a Fusion Power Plant System Based on Lead–Lithium Breeder: Comparison of the Dual-Coolant Lead–Lithium (DCLL) Blanket with the Helium-Cooled Lead–Lithium (HCLL) Concept as Initial Step," *Fusion Engineering and Design*, **84**, 2145 (2009).

6. L. El-GUEBALY, A. JABER, and S. MALANG, "State-of-the-Art 3-D Assessment of Elements Degrading the TBR of the ARIES DCLL Blanket," *Fusion Science and Technology* **61** (2012) 321-331.

7. L. EL-GUEBALY and S. MALANG, "Toward the Ultimate Goal of Tritium Self-Sufficiency: Technical Issues and Requirements Imposed on ARIES Advanced Fusion Power Plants," *Fusion Engineering and Design*, **84**, 2072 (2009).

8. P. BATISTONI, M. ANGELONE, P. CARCONI, U. FISCHER, K. FLEISCHER, K. KONDO, A. KLIX, I. KODELI, D. LEICHTLE, L. PETRIZZI, M. PILLON, W. POHORECKI, M. SOMMER, A. TRKOV, and R. VILLARI, "Neutronics Experiments on HCPB and HCLL TBM Mock-ups in Preparation of Nuclear Measurements in ITER," *Fusion Engineering and Design*, **85**, Issues 7-9, 1675 (2010).

9. "Cubit Geometry and Mesh Generation Toolkit version 12.2." Sandia National Laboratories (2010). Available at: http://cubit.sandia.gov.

10. "DAGMC Users Guide." University of Wisconsin-Madison Fusion Technology Institute (2008). Available at: http://cnerg.engr.wisc.edu/cgi-bin/index.cgi/wiki?p=DagmcUsersGuide.

11. X-5 Monte Carlo Team, "MCNP-A General Monte Carlo N-Particle Transport Code, Version 5," Vol. I, LA-UR-03-1987, Los Alamos National Laboratory (April 2003; revised 6/30/2004) and Vol. II, LA-CP-03-024S, Los Alamos National Laboratory (April 2003; revised 6/30/2004).

12. D.L. ALDAMA and A. TRKOV, “FENDL-2.1 Update of an Evaluated Nuclear Data Library for Fusion Applications,” International Atomic Agency Report INDC(NDC)-467 (2004).

13. R.N. SLAYBAUGH, P.P.H. WILSON, L.A. EL-GUEBALY, and E.P. MARRIOTT, “Three-Dimensional Source Models for Toroidal Fusion Energy Systems,” *Fusion Engineering and Design*, **84**, Issues 7-11, 1774 (2009).

14. D.K. SZE, R. CLEMMER, and E.T. CHENG, “A Novel Material for Fusion Applications,” Proc. of the 4th ANS Topical Meeting, King of Prussia, PA, Oct. 1980 (CONF80-1011, USDOE, July 1981, pp. 1786-1791). Available at: http://fti.neep.wisc.edu/pdf/fdm378.pdf.

15. P. HUBBERSTEY, T. SAMPLE, and M. BARKER, “Is Pb-17Li Really the Eutectic Alloy? A Redetermination of the Lead-Rich Section of the Pb-Li Phase Diagram (0.0 < x_{Li}(at%) < 22.1),” *Journal of Nuclear Materials*, **191-194**, 283 (1992).

16. L. EL-GUEBALY, “Three-Dimensional Neutronics Study for ARIES-ST Power Plant,” *Fusion Technology*, **34**, No. 3, 1084 (1998).

17. M.Z. YOUSSEF, N.B. MORLEY, and M. DAGHER, “Impact of the SiC FCI in the DCLL Blanket Module on the Nuclear Environment inside a Demo Reactor Configuration,” Proceedings of 23rd Symposium on Fusion Engineering, May 31–June 5, 2009, San Diego, CA, USA.

18. SHAHRAM SHARAFAT, AARON AOYAMA, NEIL MORLEY, SERGEY SMOLENTSEV, Y. KATOH, BRIAN WILLIAMS, and NASR GHONIEM, “Development Status of a SiC-Foam Based Flow Channel Insert for a U.S.-ITER DCLL TBM,” *Fusion Science and Technology*, **56**, 883 (2009).